Reducing Processing Time of Nonlinear Analysis of Symmetric-Plan Buildings

Juan C. Reyes[1]; William A. Avila[2]; Erol Kalkan, A.M.ASCE[3]; and Armando Sierra[4]

Abstract: Nonlinear response history analysis has been a powerful tool in performance-based earthquake engineering for validating the proposed design of new structures or evaluating existing ones. When it is applied to structural systems with a large number of degrees of freedom, such as three-dimensional (3D) models of tall buildings, bridges, or dams, the analyses can be time-consuming. The prolonged computing times become more prominent in parametric studies or in incremental dynamic analyses. In order to reduce the computation time, this study proposes a practical method—a reducing time steps (RTS) procedure—whereby leading and trailing weak signals in the input acceleration record are trimmed, and the remaining record is downsampled. The test results based on several different 3D computer models of reinforced-concrete idealized structures demonstrate that the RTS method is practical, and it provides estimates of engineering demand parameters such as peak values of story drift, floor acceleration, and floor velocity within 10% of the results obtained by using the original records. The RTS procedure was further validated on three symmetric-plan steel buildings with 5, 9, and 15 stories. For all analyzed cases, the average reduction in computational time was around 50%. **DOI: 10.1061/(ASCE)ST.1943-541X.0003000.** © *2021 American Society of Civil Engineers.*

Introduction

As performance-based seismic design considerations have become prerequisite for controlling the level of structural and nonstructural damage during earthquakes, the use of nonlinear response history analysis (RHA) has gained importance because it provides more accurate performance estimates of structures than nonlinear static analysis does. The RHA requires a suite of ground-motion acceleration records. For three-dimensional (3D) RHAs, pairs of seven records are often used per ASCE/SEI 7-10 (ASCE 2010), which was adopted by the 2015 International Building Code (ICC 2015) and 2016 California Building Code (ICC 2016). The required number of records was increased to 11 in ASCE/SEI 7-16 (ASCE 2016).

The nonlinear analysis can be computationally challenging and time-consuming for structural systems with a large number of degrees of freedom, such as 3D computer models of tall buildings or complex structures (e.g., dams and bridges), for ground-motion records with high sampling rates (e.g., 200 or more samples per second), and for earthquakes with long durations associated with large magnitudes (>7). The prolonged computing times become even more prominent in parametric studies or in incremental dynamic analyses (Vamvatsikos and Cornell 2002, 2004) in which a computer model of the structure is subjected to a series of nonlinear RHAs by systematically increasing the intensity of the records.

One approach to achieve computational efficiency is downsampling ground-motion records, which reduces the number of steps in the analysis. For instance, superposition of a relatively small number of pulses may be used to mimic ground-motion records; such representation is obtained by the expansion of velocity in orthogonal wavelet series using the fast wavelet transform, and approximation by only the largest energy terms in the series (Todorovska et al. 2009). Such reduced representation is useful for extracting pulses from strong motion records and for developing new algorithms for the synthesis of artificial earthquake strong motion records, but not for reducing the computational time of nonlinear RHA. This approach was not used in any way for developing the methodology proposed in this paper. In a more recent approach, filtering and downsampling were applied to the original ground-motion record. In this frequency domain method, the new sampling rate of the record is based on the frequency response function (FRF) of the structure, which is strictly valid only for linear systems (Zhong and Zareian 2014). It is evident that the complex nonlinear behavior of a multiple-story structure cannot be predicted from the transfer function of a linear system. Therefore, the approach proposed in Zhong and Zareian (2014) should be used only for linear systems. In addition, note that this proposal does not consider in any way the possibility of trimming the leading and trailing weak signals of the input acceleration record.

With the goal of obtaining a highly efficient nonlinear RHA without significant error in estimates of engineering demand parameters (EDPs), this study proposes a new hybrid approach whereby the beginning and end of the acceleration record are trimmed and the remaining record is downsampled. In this new method, the procedure proposed in Zhong and Zareian (2014) has been completely reformulated to make it applicable for nonlinear systems. This research uses a time domain formulation (rooted in structural dynamics) to develop a proxy for reducing the number of time steps. This proxy corresponds to the approximated roof displacement of the building obtained from the response of nonlinear single-degree-of-freedom (SDF) systems using a modal pushover-based approach (Chopra 2007; Chopra and Goel 2004; Reyes and Chopra 2011a, b; Reyes et al. 2015). This parameter was used to identify the leading and

[1]Associate Professor and CIMOC and Laboratory Director, Dept. of Civil and Environmental Engineering, Universidad de los Andes, Bogotá 111711, Colombia. ORCID: https://orcid.org/0000-0003-0690-2956

[2]Formerly, Master Student, Dept. of Civil and Environmental Engineering, Universidad de los Andes, Bogotá 111711, Colombia.

[3]CEO and Founder, QuakeLogic Inc., 1849 San Esteban C., Roseville, CA 95747 (corresponding author). ORCID: https://orcid.org/0000-0002-9138-9407. Email: kalkan76@gmail.com

[4]Formerly, Master Student, Dept. of Civil and Environmental Engineering, Universidad de los Andes, Bogotá 111711, Colombia.

Note. This manuscript was submitted on September 6, 2019; approved on January 6, 2021; published online on April 9, 2021. Discussion period open until September 9, 2021; separate discussions must be submitted for individual papers. This paper is part of the ***Journal of Structural Engineering***, © ASCE, ISSN 0733-9445.

trailing signals to be trimmed, and to conduct the downsampling process. Roof displacement was found to be superior to other candidates such as Arias intensity (Arias 1970) and yield base shear because it represents the characteristics of both the ground motion and structural response.

The accuracy of the proposed method was evaluated by using 3D computer models of three symmetric-plan buildings, and by comparing different EDPs estimated from the models subjected to the trimmed and downsampled records with the same EDPs obtained by subjecting the structures to the original records. The EDPs selected were story drift (i.e., interstory drift ratio), absolute peak floor acceleration, and floor velocity. The analyses were based on bidirectional excitations from a set of seven records selected and scaled according to the spectrum matching procedure (Hancock et al. 2006). The test results based on several different 3D computer models of idealized structures demonstrate that the proposed method is practical, and it provides estimates of EDPs such as peak values of story drift, floor acceleration, and floor velocity close to those obtained by using the unmodified original records. As its main contributions, this work (1) presenting, for the first time, a methodology for reducing computational time of nonlinear RHA of nonlinear systems where weak signals of the input record are removed and downsampling of the remaining time series is implemented. The method uses a time domain formulation to develop a proxy for reducing the number of time steps; (2) comprehensively evaluates the efficiency of the proposed method; and (3) develops a graphic interface application for automatically implementing the proposed methodology.

In this paper, the recommended application of the reducing time steps (RTS) procedure is limited to symmetric-plan buildings with fundamental vibration periods larger than 0.34 s. However, in a future publication, the procedure will be extended to unsymmetric-plan structures and tall buildings (Avila 2018).

Ground Motions Selected

We populated 30 ground-motion records listed in Table 1 from seven shallow crustal earthquakes with moment magnitudes 6.7 ± 0.2, at distances ranging from 20 to 30 km, and with National Earthquake Hazard Reduction Program (NEHRP) site Classification C or D (very dense soil and soft rock or stiff soil) from the Next Generation of Attenuation project database (see "Data Availability Statement"). Among them, seven records were selected for spectral matching by adding wavelets in the time domain to match the target spectrum (Hancock et al. 2006; Reyes et al. 2014). The record selection criterion was based on the difference between the target spectrum and the spectrum of each record. The selected records—identified in Table 1 with bold font—have spectral shapes close to each other. The target spectrum was defined as the design spectrum that characterizes the seismic hazard for a location in Los Angeles with NEHRP site Classification D. The number of records selected was limited to seven because previous research shows that a minimum of seven records is sufficient for unbiased estimates of EDPs from nonlinear RHAs (Reyes and Kalkan 2011, 2012). Fig. 1 depicts the 5%-damped response spectra for two horizontal

Table 1. List of ground motions

No.	Earthquake	Year	Station	Moment magnitude	Joyner-Boore distance (km)	NEHRP soil class	Ground motion no.
1	San Fernando	1971	LA–Hollywood Stor FF	6.61	22.77	D	—
2	San Fernando	1971	Santa Felita Dam (Outlet)	6.61	24.69	C	—
3	**Imperial Valley**	**1979**	**Calipatria Fire Station**	**6.53**	**23.17**	**D**	**02**
4	Imperial Valley	1979	Delta	6.53	22.03	D	—
5	Imperial Valley	1979	El Centro Array #1	6.53	19.76	D	—
6	**Imperial Valley**	**1979**	**El Centro Array #13**	**6.53**	**21.98**	**D**	**01**
7	Imperial Valley	1979	Superstition Mtn Camera	6.53	24.61	C	—
8	Irpinia, Italy	1980	Brienza	6.90	22.54	C	—
9	**Superstition Hills**	**1987**	**Wildlife Liquef. Array**	**6.54**	**23.80**	**D**	**04**
10	**Loma Prieta**	**1989**	**Agnews State Hospital**	**6.93**	**24.27**	**D**	**05**
11	Loma Prieta	1989	Anderson Dam (Downst)	6.93	19.90	C	—
12	Loma Prieta	1989	Anderson Dam (L Abut)	6.93	19.90	C	—
13	Loma Prieta	1989	Coyote Lake Dam (Downst)	6.93	20.44	D	—
14	**Loma Prieta**	**1989**	**Coyote Lake Dam (SW Abut)**	**6.93**	**19.97**	**C**	**07**
15	Loma Prieta	1989	Gilroy Array #7	6.93	22.36	D	—
16	Loma Prieta	1989	Hollister–SAGO Vault	6.93	29.54	C	—
17	Northridge	1994	Castaic–Old Ridge Route	6.69	20.10	C	—
18	Northridge	1994	Glendale–Las Palmas	6.69	21.64	C	—
19	Northridge	1994	LA–Baldwin Hills	6.69	23.51	D	—
20	Northridge	1994	LA–Centinela St	6.69	20.36	D	—
21	Northridge	1994	LA–Cypress Ave	6.69	28.98	C	—
22	Northridge	1994	LA–Fletcher Dr	6.69	25.66	C	—
23	Northridge	1994	LA–N Westmoreland	6.69	23.40	D	—
24	**Northridge**	**1994**	**LA–Pico & Sentous**	**6.69**	**27.82**	**D**	**06**
25	Kobe, Japan	1995	Abeno	6.90	24.85	D	—
26	**Kobe, Japan**	**1995**	**Kakogawa**	**6.90**	**22.50**	**D**	**03**
27	Kobe, Japan	1995	Morigawachi	6.90	24.78	D	—
28	Kobe, Japan	1995	OSAJ	6.90	21.35	D	—
29	Kobe, Japan	1995	Sakai	6.90	28.08	D	—
30	Kobe, Japan	1995	Yae	6.90	27.77	D	—

Note: Bold font indicates seven records selected for analyses. NEHRP = National Earthquake Hazard Reduction Program.

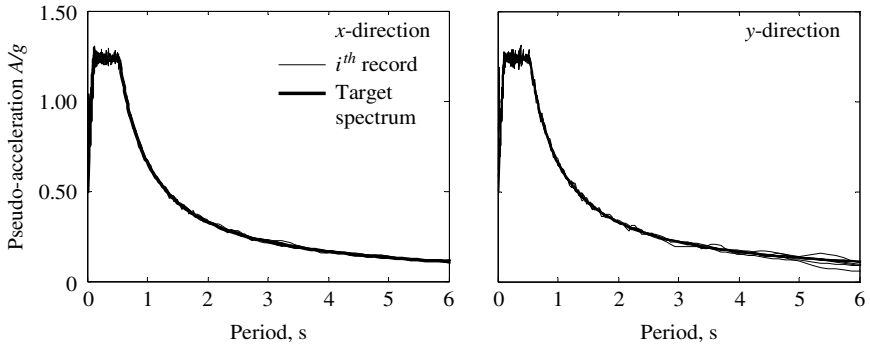

Fig. 1. Target 5% damped pseudoacceleration response spectra for seismic design of computer models in x- and y-direction. Also shown are the response spectra of seven spectral-matched records used for testing the RTS procedure.

components of the records and the 5%-damped target spectrum, which is the same in both horizontal directions. Among the three translational components of ground motion, only two horizontal components have been commonly used in the design of new or the assessment of existing structures. For this reason, vertical ground motions were excluded. Two additional seismic intensity levels were also considered by multiplying all records by global scaling factors of 0.5 and 1.50.

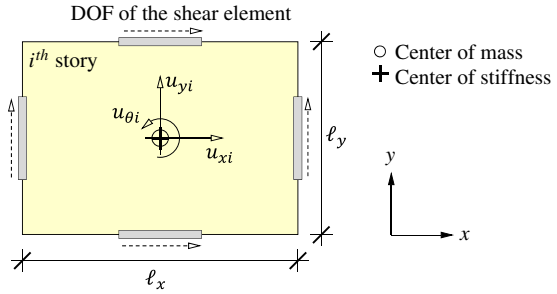

Fig. 2. Schematic plan view of structural systems where ℓ_x and ℓ_y correspond to plan dimensions; u_{xi} = translational degree of freedom in x-direction; u_{yi} = translational degree of freedom in y-direction; and $u_{\theta i}$ = rotational degree of freedom about the axis perpendicular to the plan. The lateral-load carrying structural elements are shown with their DOFs marked.

Idealized Structures

Twelve building models were created, each having a similar floor plan and floor weights, with 3, 6, 9, 12, 15, 18, 21, 24, 27, 30, 33, and 36 stories. Each structure had span lengths ℓ_x and ℓ_y of 25 m (82.02 ft), a story height of 3 m (9.84 ft), and a uniformly distributed floor load of 10 kN/m^2 (208.85 psf). The idealized structure with three main degrees of freedom (DOFs) in three dimensions (Fig. 2) was described as a shear building (stick model) containing two vertical pure-shear panels in each horizontal direction [Fig. 3(a)]. For each building plan, the center of mass (CM) coincides with the center of stiffness, as shown in Fig. 2. The structures were not reinforced concrete wall buildings, but idealized structures that represented framed systems. The structural system had a constant initial stiffness k_1 in each story (Fig. 3), which was adjusted to achieve a prescribed fundamental period T_1. Note that the fundamental period T_1 of the structures may be expressed as $T_1 = \beta\sqrt{(m/k_1)}$, where β

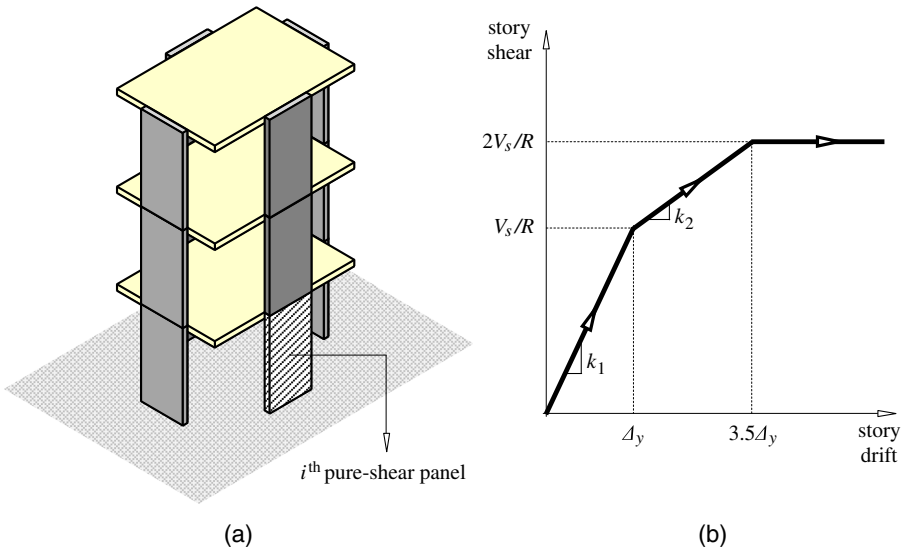

Fig. 3. (a) Three-dimensional idealized structure; and (b) story shear versus story drift where V_s = story shear; R = response modification coefficient; k_1 = initial stiffness of element; k_2 = stiffness of element in plastic range; and Δ_y = yield drift.

is a constant that depends solely on the number of stories and m is the known mass floor. The variable T_1 is defined as a function of the number of stories per Eqs. (8)–(7) in Chapter 12 of ASCE/SEI 7-10 (ASCE 2010) using the parameters for moment-resisting frames. The earthquake story shear forces (V_s) were determined by bidirectional linear response spectrum analysis of the building using the target spectrum shown in Fig. 1 for both horizontal directions. The square root of the sum of the squares (SRSS) directional combination rule was used for combining the response spectrum results in both directions. For the nonlinear analyses, a 3% damping ratio was used, as recommended by the ASCE/SEI 41-13 standard (ASCE 2013). The maximum shear force in the elastic range was estimated by dividing V_s by a response modification coefficient R equal to 3, 5, or 7 and a value that leads to linear elastic design. An over strength factor of 2.0 and an amplification factor of the yield drift Δ_y of 3.5 were selected based on actual pushover curves of frame buildings (Reyes 2009; Fajfar 2000; Medina 2002; ATC 2005). The amplification factor of yield drift is the ratio between the story drift at the maximum shear capacity ($2V_y$) and the yield drift Δ_y. This simplified model intends to represent conventional frame structures in which the lateral resisting system is located at the building perimeter. A total of 48 structures were characterized by considering different values of T_1 and R. The consideration of four response modification values R leads indirectly to various levels of inelastic demands on the idealized structures.

Procedure for Estimating Roof Displacement

Speeding up nonlinear RHA by reducing the number of time steps consists of the following steps:

1. trimming the leading weak signal,
2. trimming the trailing weak signal, and
3. downsampling the trimmed record.

Although trimming the leading weak signal may change the initial conditions of the remaining acceleration time series, such small effects are ignored because the building's dynamic response remains in the linear-elastic regime with negligible deformations during this phase. The parameter to identify the leading and trailing segments of the signal to be trimmed is the maximum roof displacement. This parameter is selected over other candidates such as the Arias intensity (Arias 1970) because it is able to represent the characteristics of both ground motion and structural response. The maximum roof displacement is estimated by implementing a modal pushover procedure based on the following theoretical background.

The system of differential equations of motion governing the response of a building subjected to bidirectional earthquake excitation, that is, ground motion along two horizontal components (x and y) applied simultaneously, is

$$\mathbf{M}\ddot{\mathbf{u}} + \mathbf{c}\dot{\mathbf{u}} + \mathbf{f}_s(\mathbf{u}) = -\mathbf{M}\boldsymbol{\iota}_x\ddot{u}_{gx} - \mathbf{M}\boldsymbol{\iota}_y\ddot{u}_{gy} \tag{1}$$

where $\mathbf{M}$ = a diagonal mass matrix; $\mathbf{c}$ = damping matrix; $\mathbf{u}$ = floor displacements vector; $\mathbf{f}_s$ = vector of resisting forces; and $\boldsymbol{\iota}_x$ and $\boldsymbol{\iota}_y$ = influence vectors associated with horizontal components $\ddot{u}_{gx}$ and $\ddot{u}_{gy}$ of the ground motion. The matrices (or vectors) $\mathbf{M}$, $\mathbf{f}_s$, $\boldsymbol{\iota}_x$, and $\boldsymbol{\iota}_y$ may be expressed in terms of submatrices (or subvectors)

$$\mathbf{M} = \begin{bmatrix} \mathbf{m} & 0 & 0 \\ 0 & \mathbf{m} & 0 \\ 0 & 0 & \mathbf{I}_o \end{bmatrix} \quad \mathbf{f}_s = \begin{bmatrix} \mathbf{f}_{sx} \\ \mathbf{f}_{sy} \\ \mathbf{f}_{s\theta} \end{bmatrix} \quad \boldsymbol{\iota}_x = \begin{bmatrix} \mathbf{1} \\ \mathbf{0} \\ \mathbf{0} \end{bmatrix} \quad \boldsymbol{\iota}_y = \begin{bmatrix} \mathbf{0} \\ \mathbf{1} \\ \mathbf{0} \end{bmatrix} \tag{2}$$

where $\mathbf{m}$ = a diagonal matrix of order N with $m_{jj} = m_j$, the mass lumped at the jth floor level; $\mathbf{I}_o$ = a diagonal matrix of order N with $I_{ojj} = I_{oj}$, the moment of inertia of the jth floor diaphragm about a vertical axis trough the CM; and $\mathbf{1}$ and $\mathbf{0}$ = vectors of dimension N with all elements equal to 1 and 0, respectively. The force-deformation relations between the displacements $\mathbf{u}_x$, $\mathbf{u}_y$, and $\mathbf{u}_\theta$ and the x-lateral forces $\mathbf{f}_{sx}$, y-lateral forces $\mathbf{f}_{sy}$, and torques $\mathbf{f}_{s\theta}$ are nonlinear and hysteretic. For one component of ground motion (say, the x-component), the floor displacements $\mathbf{u}$ at the center of mass of a linear system may be calculated as the summation of modal responses $\mathbf{u}_n$ obtained by subjecting the structure to forces $\mathbf{s}_n\ddot{u}_g$ (Chopra 2017)

$$\mathbf{u} = \sum_{n=1}^{3N} \mathbf{u}_n = \sum_{n=1}^{3N} \Gamma_n \phi_n D_n(t) \tag{3}$$

where

$$\mathbf{s}_n = \Gamma_n \mathbf{s}_n^* = \Gamma_n \begin{bmatrix} \mathbf{m}\phi_{xn} \\ \mathbf{m}\phi_{yn} \\ \mathbf{I}_\mathbf{o}\phi_{\theta n} \end{bmatrix} \tag{4}$$

$$\Gamma_n = \frac{L_n}{M_n} = \frac{\phi_n^T \mathbf{M}\boldsymbol{\iota}}{\phi_n^T \mathbf{M}\phi_n} \tag{5}$$

and $D_n(t)$ is the deformation responses of the n th-mode SDF system calculated by solving Eq. (9) for the ground motion component under consideration

$$\ddot{D}_n(t) + 2\zeta_n\omega_n\dot{D}_n(t) + \frac{F_{sn}}{L_n} = -\ddot{u}_g(t) \tag{6}$$

The subscripts x or y indicating the ground motion component are omitted in Eqs. (8) and (9), and from now on. Modal responses $\mathbf{u}_n$ are uncoupled because the displacements of a linear system to $\mathbf{s}_n\ddot{u}_g$ are completely in the nth mode. For nonlinear systems, modes other than the nth mode will contribute to the response, but researchers have demonstrated that these contributions are minor, indicating that, for this case, modes are weakly coupled (Reyes 2009; Chopra 2017). In the proposed procedure, by assuming weak modal coupling, the structure response is decomposed into its modal components using the response of nonlinear SDF systems as shown schematically in Fig. 4. Each of these SDF systems is subjected to ground accelerations $\ddot{u}_g(t)$ in order to determine its response time series $D_n(t)$. Finally, the total roof displacement is calculated by using Eq. (8).

The implemented step-by-step procedure is as follows:

1. Compute the natural frequencies ω_n (periods T_n) and modes ϕ_n of the first few N modes of linear-elastic vibration of the building. For each ground-motion component direction (x or y), identify the first modes with the largest effective modal mass (up to 90% of mass participation).
2. Develop the base shear-roof displacement, V_{bn}–u_{rn}, relation or pushover curve by nonlinear static analysis of the building subjected to the n th-mode invariant force distribution $\mathbf{s}_n^*$. Gravity loads are applied before the lateral forces, causing lateral displacement u_{rg} at the roof. This step may be implemented only for the first three modes in the direction under consideration, and may be omitted for the higher modes if their contributions to the structure's response are treated as linear-elastic.
3. Idealize the $V_{bn} - u_{rn}$ pushover curve as a bilinear or trilinear curve, as appropriate, and convert it into the force-deformation, (F_{sn}/L_n)–D_n, relation for the n th-mode equivalent inelastic SDF system using well-known relationships

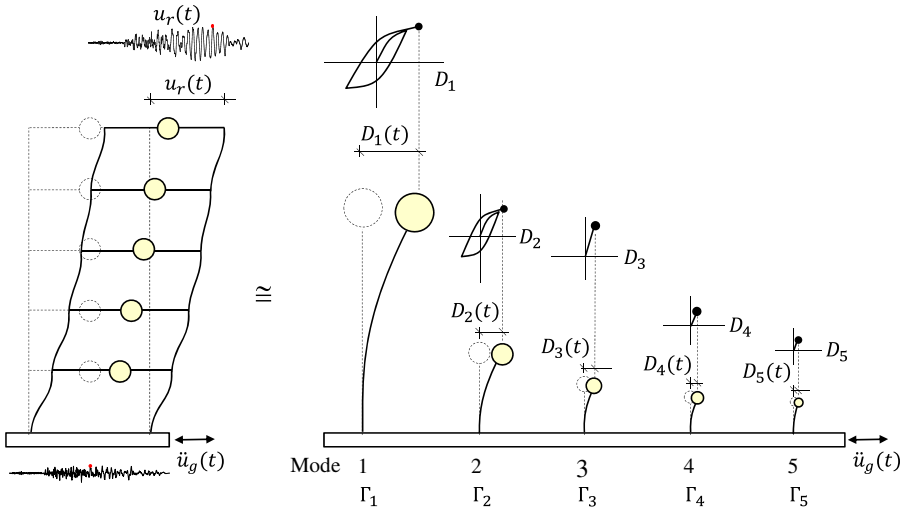

Fig. 4. Schematic representation of the modal pushover-based procedure used to estimate peak roof displacement.

$$\frac{F_{sn}}{L_n} = \frac{V_{bn}}{M_n^*} \quad \text{and} \quad D_n = \frac{u_{rn} - u_{rg}}{\Gamma_n \phi_{rn}} \tag{7}$$

where F_{sn} = a nonlinear hysteretic function of the nth modal coordinate; M_n^* = effective modal mass for the nth mode; and ϕ_{rn} = value of ϕ_n at the CM of the roof. Starting with this initial loading curve, define the unloading and reloading branches appropriate for the structural system and material being considered as follows:

4. Compute deformation $D_n(t)$ for the n th-mode inelastic SDF due to the input record by solving Eq. (9).
5. Compute the roof displacement of the nth mode in the direction under consideration

$$u_{rn}(t) = \Gamma_n \phi_{rn} D_n(t) \tag{8}$$

6. Compute the total roof displacement in the direction under consideration

$$u_r = \sum_{n=1}^{N} u_{rn}(t) \tag{9}$$

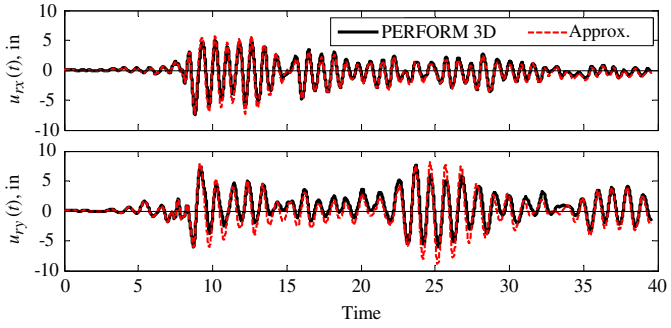

Fig. 5. Comparison of approximate roof displacement from modal pushover-based analysis and exact roof displacement from nonlinear response history analysis using PERFORM 3D. The results correspond to the 9-story symmetric-plan (R09) building subjected to ground motion GM01. Note the matching time history results.

7. Implement Steps 4–6 for the orthogonal horizontal component of ground motion and estimate the final roof displacement.

Fig. 5 shows a representative comparison between the time history of the roof displacement of a 9-story building computed by formal nonlinear RHA using PERFORM 3D version 6.0, and by the modal pushover-based procedure described previously. The estimated roof displacement time series are practically similar to those obtained from nonlinear RHA. The difference in peak values is less than 10%. Other records yielded similar differences.

Reducing Time Steps Procedure for Modifying Ground-Motion Records

The proposed ground-motion modification method for reducing the number of time steps of the RHA is composed of three steps. Each step requires the computation of time histories of roof displacement by using an equivalent nonlinear-inelastic SDF system considering two horizontal components (x and y) of the record. These steps are as follows:

1. Remove the leading weak signal from the original record. The leading weak signal that includes the pre-event interval starts from the beginning of the record to the last zero crossing before the roof displacement (u_r) reaches an initial target roof displacement (u_{ri}) defined as

$$u_{ri} = f_i \cdot \max(|u_r(t)|) \tag{10}$$

where f_i = displacement modification factor for the leading signal; and | | = absolute value operator. The value of u_r is computed by implementing Eq. (12). Identification of the leading weak signal is illustrated in Fig. 6. Fig. 6(a) shows the input acceleration record and Fig. 6(b) displays the roof displacement u_r. The variable f_i can be taken as 10% (as explained in the "Results from Idealized Structures" section).

2. Remove the trailing weak signal. The trailing weak signal starts from a time instant when the roof displacement (u_r) reaches a final target roof displacement (u_{rf}) and ends at the termination of the record. The variable u_{rf} is defined as

$$u_{rf} = f_f \cdot \max(|u_r(t)|) \tag{11}$$

where f_f = displacement modification factor for the trailing signal. Identification of the trailing weak signal is illustrated in

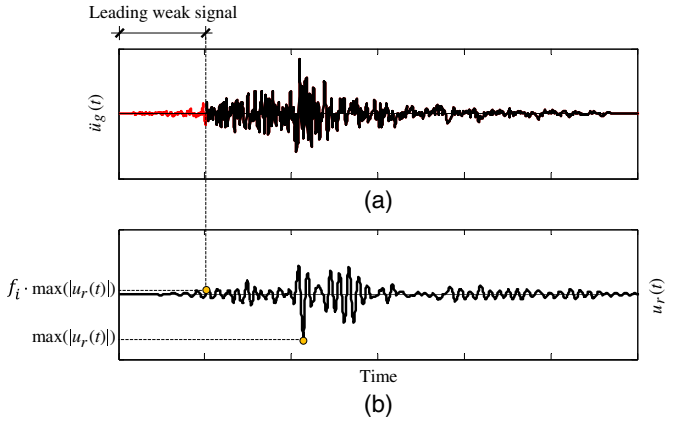

Fig. 6. (a) Trimming the leading weak signal from the ground-motion acceleration record using the (b) modified peak roof displacement value, estimated from the equivalent nonlinear-inelastic SDF system, as a proxy. Maximum roof displacement and its value modified by f_i are marked with circles.

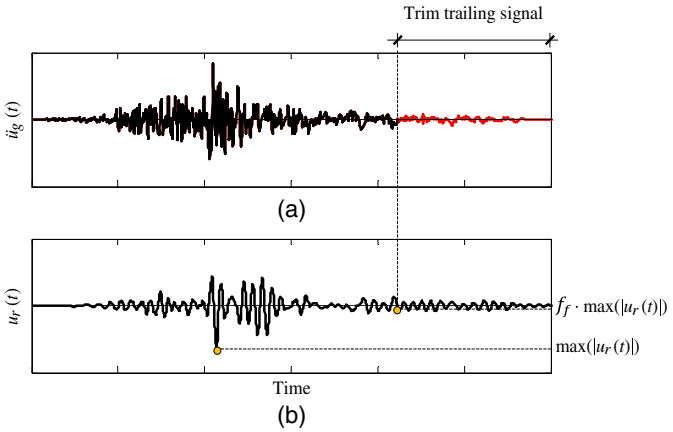

Fig. 7. (a) Trimming the trailing weak signal from the ground-motion acceleration record using the (b) modified peak roof displacement value, estimated from the equivalent nonlinear-inelastic SDF system, as a proxy. Maximum roof displacement and its value modified by f_f are marked with circles.

Fig. 7. The value of f_f can be taken as 20% (as explained in the "Results for Idealized Structures" section).

3. The downsampling is performed by adapting the procedure in Todorovska et al. (2009) as follows:
   a. Transform the roof displacement time series into frequency domain by fast Fourier transform (FFT).
   b. Identify the largest frequency ($\omega_{1\%}$) associated with amplitude at least 1% of the peak response.
   c. Apply a low-pass filter to the trimmed record with cutoff frequency $\omega_{\text{cut}} = \omega_{1\%}/f_m$, where f_m is a modification factor that modifies the usable frequency range.
   d. Modify time step dt as a multiple of 0.005 s (200 samples per second) less than or equal to π/ω_{cut}.
   e. Resample the filtered record by picking every mth sample, where m represents the new sampling rate defined as the rate of the new and the original time step. An example is illustrated in Fig. 8 showing the correspondence between the original and downsampled records. The value of f_m can be taken as 10% (as explained in the "Results for Idealized Structures" section).

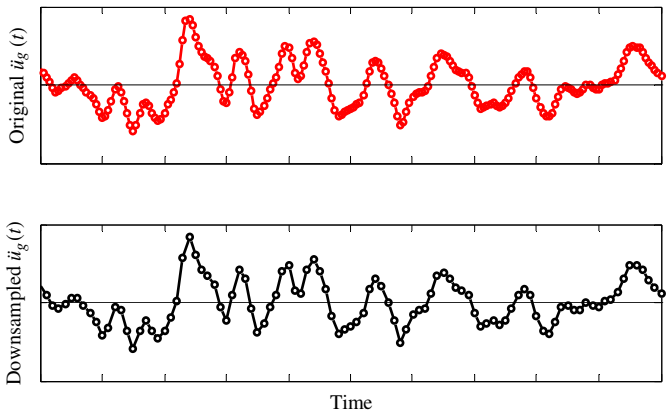

Fig. 8. Reducing the sampling rate of a ground-motion acceleration record. The results correspond to a structure with fundamental period of 1.18 s with response modification factor $R = 5$ subjected to ground motion GM01. The initial sampling rate is 200 samples per second (sps), and the final sampling rate is 100 sps.

It is clear that the success of the procedure depends on the value of the modification factors, f_i, f_f, and f_m.

Results from Idealized Structures

This study seeks to identify an appropriate and efficient trimmed segment length for trailing and leading weak signals and the optimum time step for the remaining record, given a ground motion and structural system, to ensure that there will be enough data in the record to execute a nonlinear RHA with a small and stable error.

First, we examined the effects of trimming and downsampling on the accuracy of the nonlinear RHA results. The f_i and f_m parameters varied from 2.5% to 50% in 2.5% intervals, and the f_f parameter varied from 5% to 75% in 5% intervals. The parametric study, covering a wide range of values for modification factors, was conducted using seven modified records for 48 different structural systems with four different design strength (R) values and 12 different fundamental periods (T_n). In total, 18,816 RHAs were conducted. The procedure for establishing the appropriate trimmed segment length for trailing and leading weak signals and the optimum time step was evaluated in terms of the error in EDPs obtained from original and modified records. The EDPs selected are the maximum observed story drift, absolute peak floor acceleration, and floor velocity.

Fig. 9 presents the relative error in story drift. In this figure, each column shows the results for the structures characterized by R, and each row presents the results for one of the modification factors. The values on the horizontal axis of each subplot represent T_n. The value bar represents the relative error (in percentage) associated with each contour. For each structure, the percent error was calculated using the median of the peak drift values coming from the seven records considered. As expected, the error in peak story drift becomes larger as the value of f_i increases because it leads to a longer segment of the record to be trimmed. The error also depends proportionally on the modification coefficient f_m, because a larger f_m generates a larger time step (reduced sample size). In contrast, trimming the trailing weak signal results in no error in the peak story drift estimates because this modification occurs after the instant of the peak story drift. There is no clear correlation between

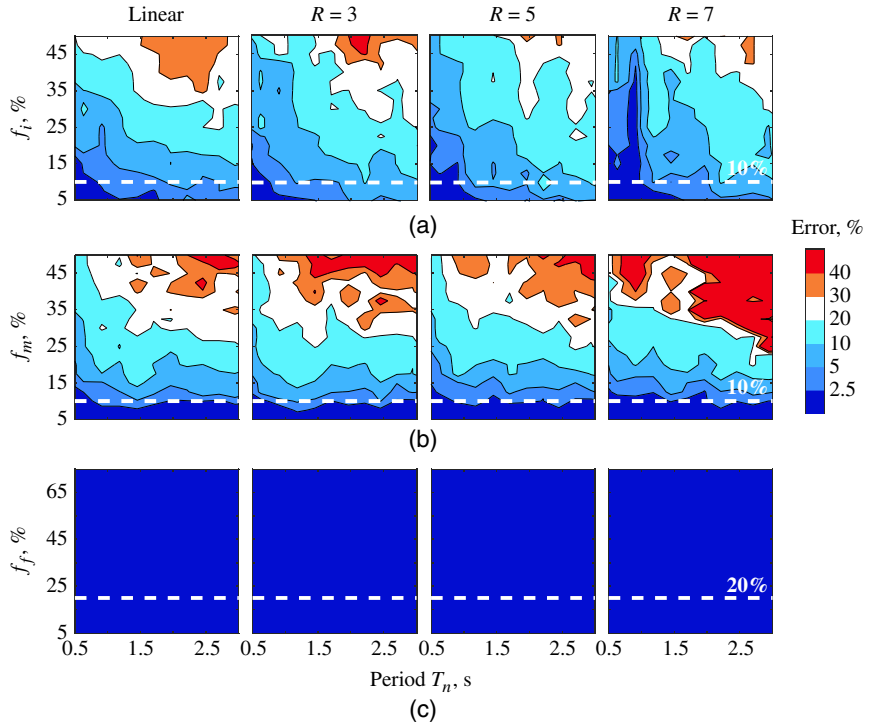

Fig. 9. Percent error in peak story drift as a function of fundamental period (T_n) and ground-motion modification factors: (a) f_i for trimming the leading weak signal; (b) f_m for downsampling the signal; and (c) f_f for trimming the trailing weak signal. The results are based on seven selected ground-motion records shown in Fig. 1 considering 12 fundamental periods ($T_n = 0.34$–3.18 s) and four response modification coefficients (R = linear, 3, 5, and 7). The horizontal white dashed lines indicate the proposed values of f_i, f_m, and f_f.

the error in peak story drift and the response modification coefficient. The error generated by trimming the leading weak signal and by downsampling appears to be higher for structures with long periods ($T_n \geq 1$ s) as compared to the error for structures with short periods ($T_n < 1$ s). For example, for $f_i = 25\%$, the error can reach 5% for structures with $T_n = 1$ s, whereas the error can be as high as 20% for structures with $T_n = 2.5$ s. Similarly, for $f_m = 25\%$, the error for a structure with $T_n = 1$ s would be 10%, whereas it would be as high as 20% for a structure with $T_n = 2.5$ s. In general, the error is less than 5% for f_i from 0% to 10% and for f_m from 0% to 15%.

Fig. 10 presents the relative error in absolute peak floor velocity. Again, there is no clear correlation between R and the relative error. The effect of T_n on the error in the estimation of the EDP varies; in some cases, it appears to be random (e.g., in the subplot for trimming the leading weak signal with $R = 5$). Trimming the trailing weak signal has no negative effect on the estimation of the EDP. As the values of f_i and f_m increase, the error in the estimates of EDP increases. An appropriate value, yielding relative error within 2.5%, for both f_i and f_m is found to be between 0% and 15%.

Fig. 11 portrays the relative error in absolute peak floor acceleration. The error for this EDP presents almost same distributions as that for the other two EDPs in Figs. 8 and 9 with respect to R, T_n, and the modification factors f_i and f_f. The absolute peak floor acceleration is more sensitive to f_m. The appropriate value for f_m should be limited to 10% in order to limit the error within 5%.

Fig. 12 displays the time steps and computational time saved. By trimming the leading weak signal with $f_i = 10\%$ (as defined previously), the time efficiency could be up to 10%, which may not be a large portion of the original record but it does not change with T_n. Reduction of the sampling rate is the most effective method for time efficiency because the definition of a new time step implies that the number of data points in the ground motion will be divided by an integer greater than or equal to 1, which should lead to a reduction of at least 50% in time steps. By trimming the trailing weak signal with various values of f_f (5%–50%) [Fig. 12(c)], the reduction in time steps varies from 5% to 40% of the original time steps. In this case, time efficiency is dependent on T_n. Savings in computational time are greater than 60% for most low-R structures, and around 50% for structures with $R = 5$ and 6. However, for the shortest period analyzed (0.34 s) the savings in time steps and run time are minor.

The figure shows that for structures with periods between 0.63 and 1.18 s, the number of time steps saved by f_f is higher than in those with longer periods ($T_n \geq 1.45$ s). This is expected because the structures with long periods undergo free vibration in longer duration, and in consequence no trailing weak signals are present in the roof displacement time series. This fact creates a limitation because it is not possible to ensure that the residual displacements can be estimated correctly. However, even for the original records, estimating residual displacements may require adding additional zeros at the end of the record to continue the analysis and let the structure freely vibrate until it eventually stops. The selection of the appropriate value of f_f should be based only on the desired reduction of the record's trailing segment. Trimming the trailing weak signal does not introduce any error in the estimation of different EDPs, as shown in Figs. 9–11, because this particular modification occurs after the instant of the peak. To be on the conservative side, f_f is assumed to be 20%, which may reduce the time steps as much as 30%, as shown by dashed line in Fig. 12(c).

Fig. 13 demonstrates the combined effects of proposed values of f_i, f_m, and f_f (marked in Fig. 12 with dashed lines) on the error in

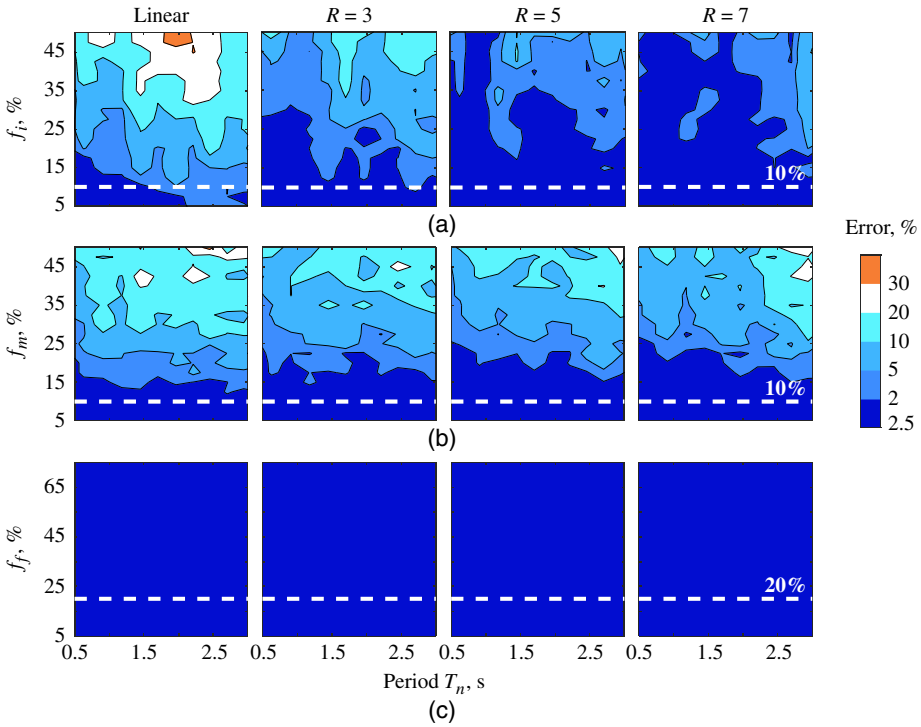

Fig. 10. Percent error in peak absolute roof velocity as a function of fundamental period (T_n) and ground-motion modification factors: (a) f_i for trimming the leading weak signal; (b) f_m for downsampling the signal; and (c) f_f for trimming the trailing weak signal. The results are based on seven selected ground-motion records shown in Fig. 1 considering 12 fundamental periods ($T_n = 0.34$–3.18 s) and four response modification coefficients (R = linear, 3, 5, and 7). Trimming the trailing weak signal results in no error in the estimation of the peak demand value because this particular modification occurs after the instant of the peak. The horizontal white dashed lines indicate the proposed values of f_i, f_m, and f_f.

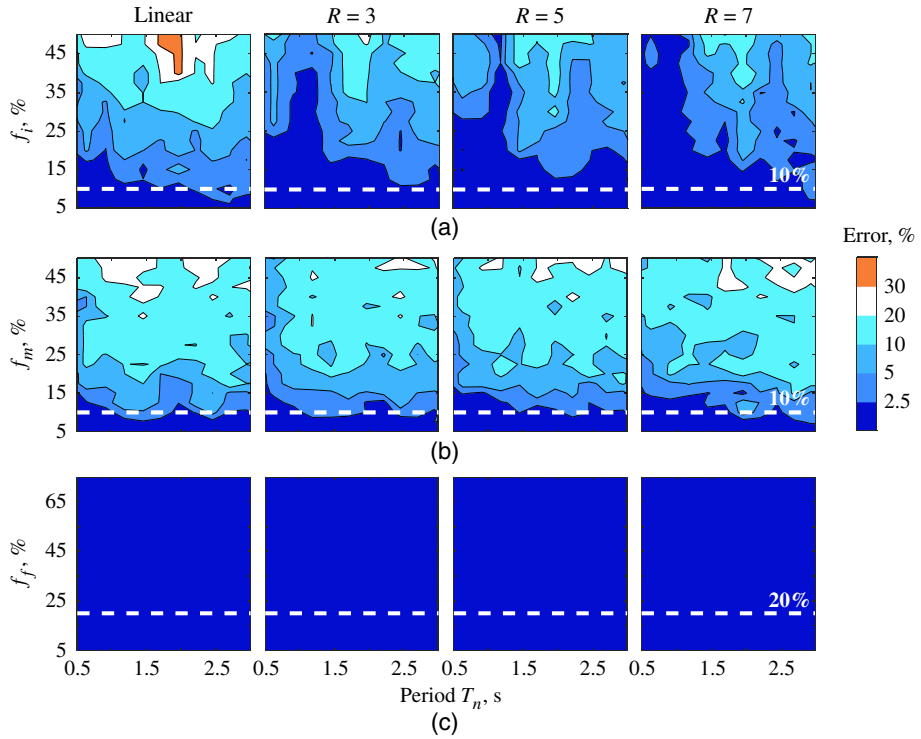

Fig. 11. Percent error in peak absolute roof acceleration as a function of fundamental period (T_n) and ground-motion modification factors: (a) f_i for trimming the leading weak signal; (b) f_m for downsampling the signal; and (c) f_f for trimming the trailing weak signal. The results are based on seven selected ground-motion records shown in Fig. 1 considering 12 fundamental periods ($T_n = 0.34$–3.18 s) and four response modification coefficients (R = linear, 3, 5, and 7). The trimming trailing weak signal results in no error in the estimation of the peak demand value because this particular modification occurs after the instant of the peak. The horizontal white dashed lines indicate the proposed values of f_i, f_m, and f_f.

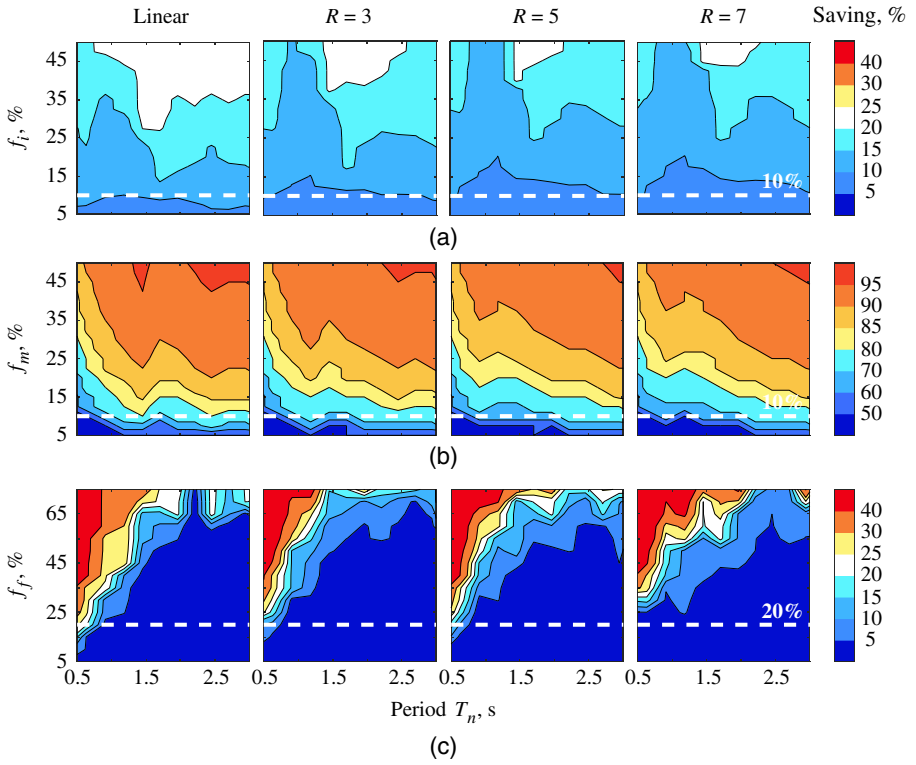

Fig. 12. Percent reduction in time steps using modified records as a function of the fundamental period (T_n) and ground-motion modification factors: (a) f_i for trimming the leading weak signal; (b) f_m for downsampling the signal; and (c) f_f for trimming the trailing weak signal. The results are based on seven selected ground-motion records shown in Fig. 1 considering 12 fundamental periods (T_n = 0.34–3.18 s) and four response modification coefficients (R = linear, 3, 5, and 7). The horizontal white dashed lines indicate the proposed values of f_i, f_m, and f_f.

the peak roof displacement estimates, and the contribution of these modification factors on the total time steps saved. For the proposed values of $f_i = f_m = 10\%$, and $f_f = 20\%$, the error is within 5% for almost all cases, and the average reduction in time steps is 70% as compared to the original records. For structures with shorter fundamental periods (e.g., $T_n \leq 0.91$ s), the time step reduction is mainly due to trimming of the leading and trailing signals. For structures with longer fundamental periods ($T_n \geq 1.18$ s), the reduction is mainly due to downsampling the record. This is the benefit of using three different criteria when modifying the ground-motion records. Note that the proposed values are based on the specific cases studied herein and other scenarios not shown here (Avila 2018 . Table 2 shows a summary of EDP values (base shear, roof displacement, and story drift) obtained from the original records and their corresponding errors when the RTS procedure is applied for $f_i = 10\%$, $f_m = 10\%$, and $f_f = 20\%$. Reported benchmark values are the median of the peak EDP quantities coming from the seven records for structures with $R = 5$. A minus sign in the percent error indicates underestimation of the EDPs. It is evident that for most cases the errors are very small, confirming the robustness of the RTS procedure.

The means of the peak drift values are similar to those obtained from the original records, as demonstrated by the results of the analysis of variance (ANOVA) shown in Table 3. The ANOVA test returns the value under the null hypothesis that both RTS and the original results are drawn from populations with the same mean. If p is near zero, it questions the null hypothesis and suggests that the means of RTS EDP values are significantly different from those obtained from the original records. For most cases, this statistical test shows p values well above the typical significance level of 0.05 (commonly used in these tests). In general, p values decrease for long period structures designed for low R values, but no value is below 0.05.

To evaluate the effect of the RTS procedure in the estimations of structural cyclic performance, the effective number of cycles N_{cy} and the cumulative ductility factor η were calculated for the story with the largest drift values using the following equations (Akiyama 1985; Malhotra 2002):

$$N_{cy} = \frac{1}{2}\sum\left(\frac{\Delta_i}{\Delta_{\max}}\right)^2 \tag{12}$$

$$\eta = \frac{E_D}{V_y\Delta_y} = \frac{\int V d\Delta - V^2/2k_1}{V_y\Delta_y} \tag{13}$$

where Δ_i = amplitude of the ith drift half cycle; $\Delta_{\max}$ = amplitude of the largest drift half cycle; V = story shear; and E_D = energy dissipated by yielding. Table 4 shows peak values of N_{cy} and η as representative results for the original records together with the percent error of RTS estimations for structures with $R = 5$. Note that, in general, errors are within the 5% range.

Validation Based on Actual Building Models

The structures considered for the validation of the proposed method were three symmetric-plan steel buildings with 5, 9, and 15 stories characterized by T_n of 1.03, 1.51, and 2.51 s, respectively. The lateral load resisting system of these structures consisted of ductile steel moment frames in the longitudinal and transverse directions. These buildings were designed according to the 2016 California Building Code (ICC 2016) to be located in Los Angeles, California. Their plan

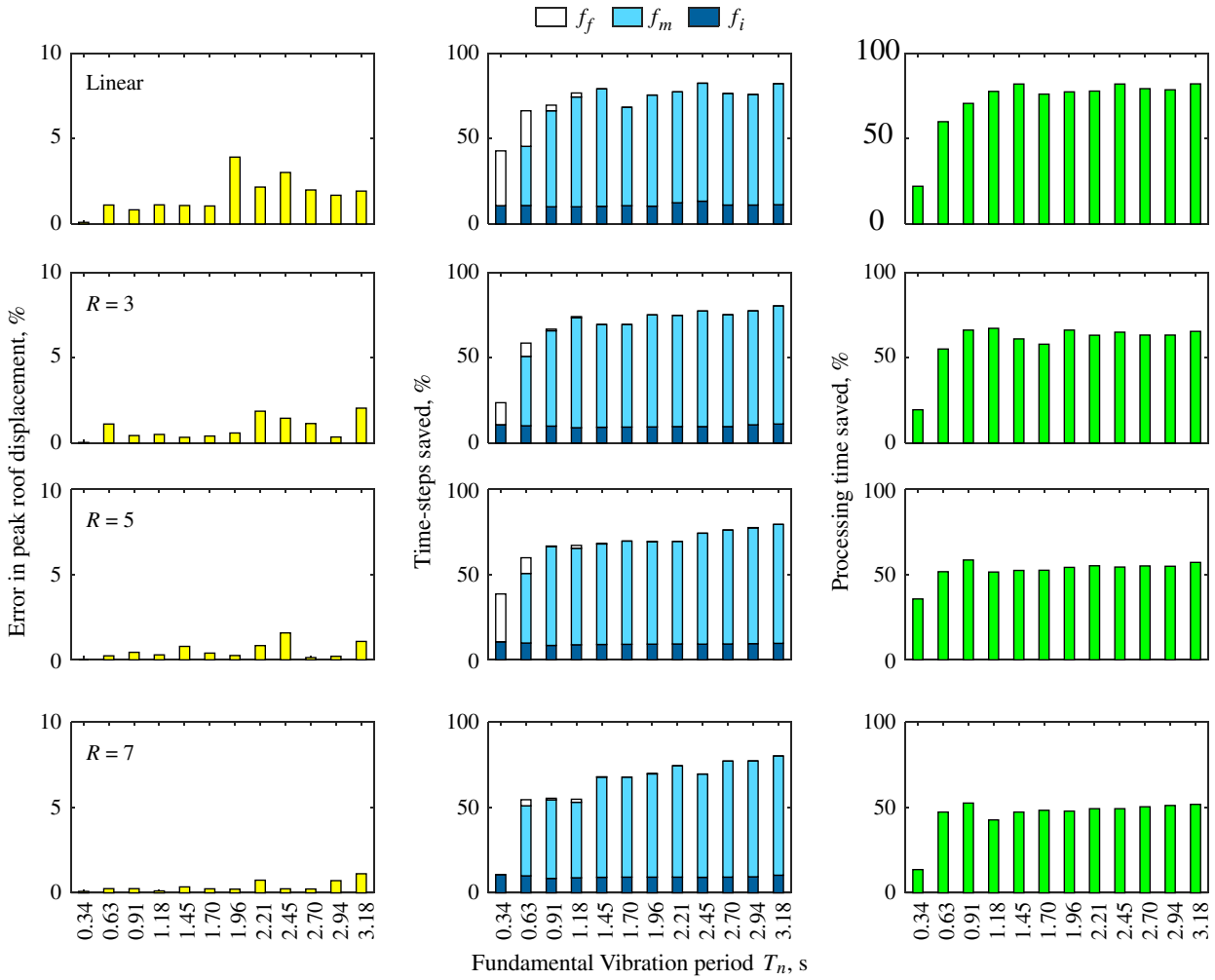

Fig. 13. (a) Percent error in peak roof displacement by using modified records as compared to the original records; (b) time steps saved; and (c) processing time savings by using the RTS procedure. Results are based on final values of ground-motion modification factors f_i, f_f, and f_m.

Table 2. Peak benchmark EDPs and RTS procedure errors for idealized and realistic structures

Structure type	Fundamental period of vibration, T_n (s)	EDP values obtained from the original records: Base shear (kN)	Roof displacement (mm)	Story drift (%)	Percentage of error in EDP estimations for $f_i = 0.10$, $f_m = 0.10$, and $f_f = 0.20$: Base shear	Roof displacement	Story drift
Idealized structures $R = 5$	0.34	14,675	46	2.18	−0.01	0.00	−0.01
	0.63	23,722	135	3.56	−0.08	2.31	0.16
	0.91	21,738	168	2.97	1.55	−1.05	2.54
	1.18	23,086	221	3.11	−0.18	−1.38	−0.30
	1.45	23,220	259	3.08	−0.32	−0.17	−0.53
	1.70	25,146	292	3.28	−0.23	−0.34	−0.37
	1.96	25,288	356	3.22	0.00	−0.26	−0.01
	2.21	25,373	391	3.19	−0.08	1.35	0.52
	2.45	23,820	442	2.77	−0.09	0.21	−0.13
	2.70	25,591	500	3.03	−0.07	−2.21	−0.16
	2.94	23,905	594	2.75	−0.23	−0.21	−0.10
	3.18	25,035	643	2.91	0.14	−6.19	−4.15
Actual building models	1.03 (R05)	31,138	218	1.83	−0.09	1.52	−0.20
	1.51 (R09)	25,866	356	1.49	−0.76	−0.64	−0.25
	2.51 (R15)	57,102	475	1.57	−0.16	0.36	0.48

Table 3. Results of ANOVA significance tests for estimation of peak story drifts of idealized structures

Fundamental period of vibration, T_n (s)	p values from ANOVA test for peak story drift			
	Linear	$R = 3$	$R = 5$	$R = 7$
0.34	0.977	0.952	0.993	0.988
0.63	0.976	0.943	0.992	0.994
0.91	0.782	0.999	0.973	0.938
1.18	0.891	0.974	0.949	0.870
1.45	0.997	0.924	0.998	0.999
1.70	0.862	0.882	0.792	0.951
1.96	0.996	0.749	0.779	0.942
2.21	0.893	0.960	0.919	0.823
2.45	0.728	0.901	0.739	0.884
2.70	0.125	0.879	0.917	0.946
2.94	0.539	0.816	0.843	0.931
3.18	0.682	0.523	0.478	0.699

Table 4. Number of cycles N_{cy} and cumulative ductility factors η obtained for idealized structures with $R = 5$ subjected to the original records, including RTS estimate error

Fundamental period of vibration, T_n (s)	Original records		Percent error for $f_i = 0.10$, $f_m = 0.10$, and $f_f = 0.20$	
	N_{cy}	η	N_{cy}	η
0.34	4.7	10.8	−1.79	−2.44
0.63	3.7	5.1	−0.96	1.87
0.91	5.0	5.7	−0.13	2.82
1.18	4.5	7.3	−0.34	−1.18
1.45	3.8	6.1	0.63	1.52
1.70	3.7	6.3	−3.64	−2.36
1.96	3.4	6.1	−1.88	−4.65
2.21	3.0	7.3	−8.82	−0.30
2.45	2.9	6.3	−0.19	2.38
2.70	2.4	5.0	−3.94	−3.95
2.94	2.0	5.9	−1.03	2.64
3.18	2.3	6.0	−1.16	−3.11

shapes are shown in Fig. 14, where the perimeter moment-resisting frames are highlighted with thick lines. The buildings are identified by the letter R, which stands for quasi-rectangular, followed by the number of stories. The buildings have similar square footage and floor weights. The earthquake design forces were determined by bidirectional linear response spectrum analysis of the buildings with the design spectrum reduced by a response modification factor $R = 8$. However, member sizes were governed by drift limits instead of strength requirements.

The nonlinear RHAs and pushover analyses were conducted using PERFORM 3D version 6.0. The following features were used in the modeling:

1. Girders and columns were modeled by a linear element with trilinear plastic hinges at the elements' ends that can include in-cycle strength deterioration, but not cyclic stiffness degradation; axial load-moment interaction for the columns was based on plasticity theory.
2. Panel zones were modeled as four rigid links hinged at the corners with a rotational spring that represents the strength and stiffness of the connection.
3. Ductility capacities of girders, columns, and panel zones were specified according to the ASCE/SEI 41-13 standard (ASCE 2013).
4. Columns of moment-resisting frames were assumed to be fixed at the base, whereas gravity columns were considered pinned at the base.
5. Effects of nonlinear geometry were approximated by a standard P–Δ formulation for both moment and gravity frames. A 3% damping ratio was used as recommended by the ASCE/SEI 41-13 standard (ASCE 2013).

The structures were subjected to the seven selected records shown in Fig. 1. The objective was to compare the EDPs calculated by using the original and modified records. Fig. 15 shows the story drift, absolute peak velocity, and acceleration values at the corner column of each building (Fig. 14). Fig. 15(a) displays the EDPs in the x-direction; Fig. 15(b) shows the EDPs in the y-direction. The markers and horizontal lines represent the median and the 25th and 75th quartiles of the EDP for the modified records using $f_i = 10\%$, $f_m = 10\%$, and $f_f = 20\%$. For comparison, the 25th and 75th quartile of each EDP from the original records are presented in all subplots as a gray shaded area. Table 2 shows a summary of EDP values (base shear, roof displacement, and story drift) obtained from the original records and their corresponding errors when the RTS procedure is applied. From Fig. 15 and Table 2, it is evident that the RTS procedure leads to accurate EPD estimations keeping the errors within the 5% range.

Fig. 16 presents the results for the shear force computed at the girder and column identified in Fig. 14. The effects of the ground-motion modification on these EDPs are negligible. The dispersion of the EDPs is very small for both original and modified records. The median values in each story are almost exact. Fig. 17 displays the time steps saved for each building; the average reduction in time steps was 53%, 60%, and 71% for buildings R05, R09, and R15, respectively. Average savings in computational time was around 50% for these buildings. Larger run-time savings may be achieved by selecting greater values of f_i, f_m, and f_f.

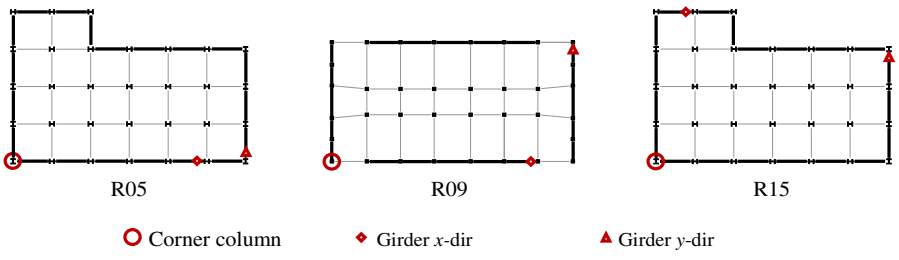

Fig. 14. Plan views of 5-, 9-, and 15-story symmetric-plan (denoted by R) steel buildings. Thick black lines highlight the perimeter moment-resisting frames. The marked locations with circles, diamonds, and triangles respectively indicate joints, girders, and columns where the critical engineering demand parameters are in effect.

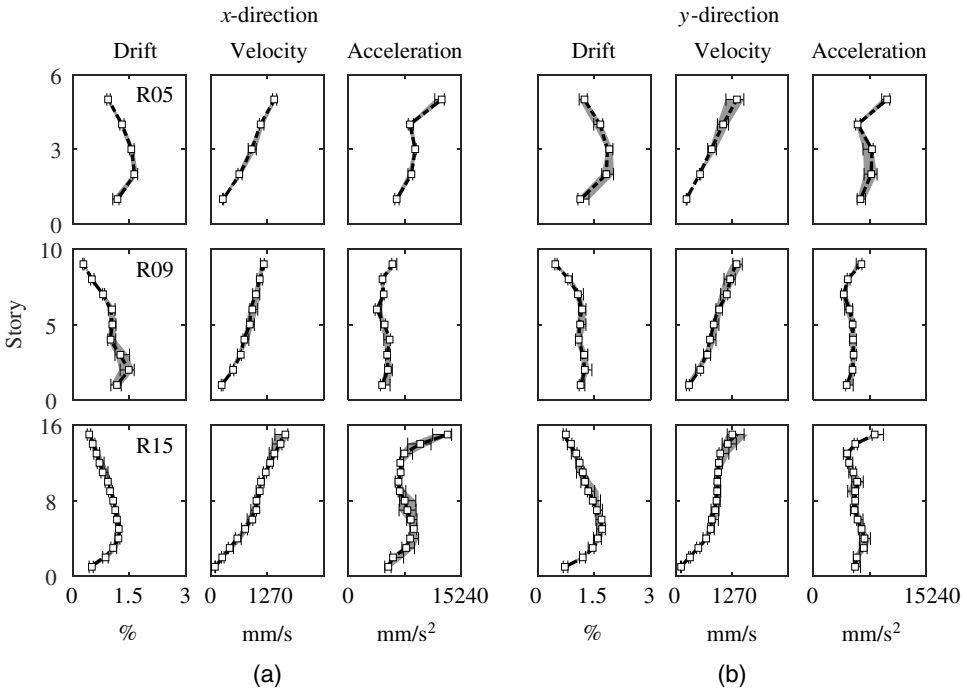

Fig. 15. Drift (interstory drift ratio), absolute peak floor velocity, and acceleration in (a) the x-direction; and (b) the y-direction for 5-, 9-, and 15-story symmetric-plan buildings (Fig. 14). In each panel, the marker and horizontal line represent the median and 25th and 75th quartiles (gray shaded area) of the EDP.

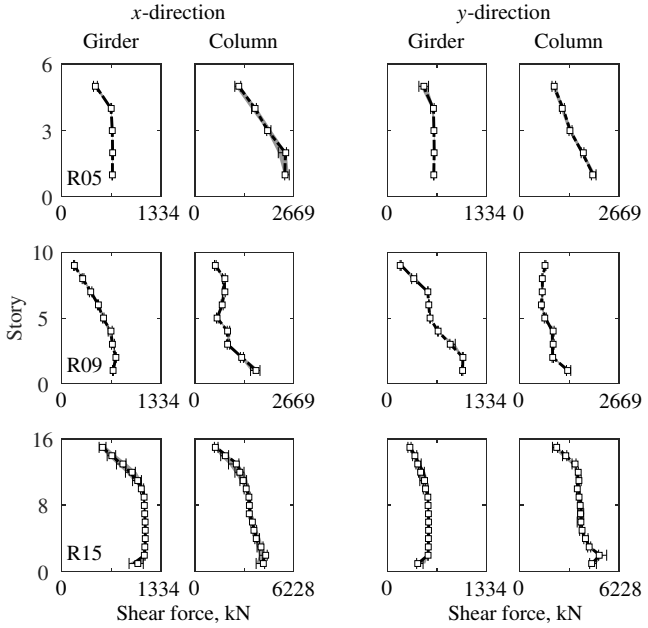

Fig. 16. Girder and column shear force in x- and y-direction for 5-, 9- and 15-story symmetric-plan buildings (Fig. 14). In each panel, the marker and horizontal line represent the median and the 25th and 75th quartiles (gray shaded area) of the EDP.

Additional Seismic Intensities

The RTS procedure was also tested using two additional seismic intensities obtained by applying scaling factors of 0.5 and 1.5 to the original ground motions. The EDPs (peak base shear, roof displacement, and story drift) obtained from this new set of analyses are shown in Table 3 for the idealized structures with $R = 5$ and for the R05, R09, and R15 structures. Building R09 presented numerical convergence problems (NCP) when it was subjected to ground motions scaled by a factor of 1.50. Note that for all cases shown in Table 5, errors were less than 5%, indicating the accuracy of the proposed procedure in estimating EDPs for the two additional seismic intensities tested.

Conclusions

In this article, the RTS procedure is proposed to achieve fast nonlinear response history analyses (RHAs) of symmetric-plan building structures with fundamental vibration periods above 0.34 s. In this procedure, ground-motion records are represented by a relatively short duration (by removing leading and trailing weak signals) and a reduced sampling rate considering the characteristics of both the ground motion and structural response. The procedure was tested comprehensively by using 48 idealized structure models within a parametric study as well as by using three realistic building models. The following conclusions were drawn:

- The RTS procedure was shown to be effective in limiting the error in EDPs (including story drift, floor acceleration, floor velocity, girder shear, and column shear). The median values of EDPs from the set of seven records were not affected by the reduction in the number of time steps. The dispersion values of the EDPs were slightly increased for some cases, which is acceptable because they lead to conservative results.
- The average savings in computational run time were about 50% for most buildings analyzed.

For estimating residual displacements, computational times may be elongated because additional zeros at the end of the record must

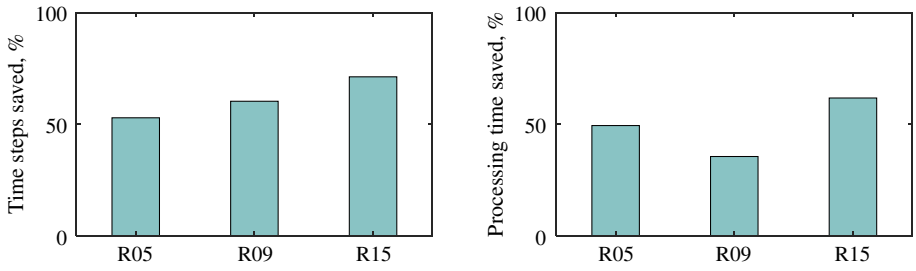

Fig. 17. Percent ratio of time steps between modified and original records. The results are for symmetric-plan (denoted by R) 5-, 9-, and 15-story buildings (Fig. 14) considering the seven ground motions shown in Fig. 1.

Table 5. Peak benchmark EDPs and RTS procedure errors for two additional seismic intensities

Structure type	Fundamental period of vibration, T_n (s)	EDP values obtained from original records: Base shear [kN (kip)]	Roof displacement [mm (in.)]	Story drift (%)	Percent error in EDP estimations for $f_i = 0.10$, $f_m = 0.10$, and $f_f = 0.20$: Base shear	Roof displacement	Story drift
Idealized structures, $R = 5$, scaling factor = 0.5	0.34	10,226 (2,299)	25 (1.0)	1.17	−0.04	−1.28	−0.07
	0.63	16,623 (3,737)	74 (2.9)	1.93	0.72	0.38	1.43
	0.91	16,587 (3,729)	102 (4.0)	1.83	0.53	−1.03	1.08
	1.18	17,384 (3,908)	142 (5.6)	1.88	0.35	1.74	0.70
	1.45	17,695 (3,978)	165 (6.5)	1.79	−1.60	−0.11	−3.27
	1.70	18,549 (4,170)	191 (7.5)	1.93	0.62	1.20	1.24
	1.96	19,114 (4,297)	211 (8.3)	1.94	−0.55	5.34	−1.53
	2.21	18,749 (4,215)	254 (10.0)	1.87	0.35	−0.15	0.71
	2.45	18,865 (4,241)	274 (10.8)	1.87	1.36	−0.26	4.77
	2.70	18,705 (4,205)	302 (11.9)	1.65	−1.99	0.02	−3.71
	2.94	19,083 (4,290)	340 (13.4)	1.73	−1.43	0.75	−2.57
	3.18	19,158 (4,307)	371 (14.6)	1.69	−0.05	−1.23	−0.11
Actual building models, scaling factor = 0.5	1.03 (R05)	24,545 (5,518)	145 (5.7)	1.20	−3.42	−0.03	−0.67
	1.51 (R09)	19,029 (4,278)	203 (8.0)	0.78	4.11	1.23	0.14
	2.51 (R15)	42,231 (9,494)	320 (12.6)	1.05	−3.05	−0.52	−0.78
Idealized structures, $R = 5$, scaling factor = 1.5	0.34	16,961 (3,813)	76 (3.0)	3.53	0.00	0.00	−0.44
	0.63	27,686 (6,224)	196 (7.7)	5.16	0.00	2.85	2.96
	0.91	26,187 (5,887)	259 (10.2)	4.03	−0.43	0.09	0.04
	1.18	29,456 (6,622)	325 (12.8)	4.63	0.00	0.73	−0.81
	1.45	30,208 (6,791)	389 (15.3)	4.76	0.00	−0.48	0.55
	1.70	30,951 (6,958)	404 (15.9)	4.90	−0.31	−0.26	0.30
	1.96	31,262 (7,028)	500 (19.7)	4.47	−0.61	0.02	−0.11
	2.21	31,080 (6,987)	599 (23.6)	4.31	−0.05	0.09	−0.07
	2.45	29,781 (6,695)	632 (24.9)	3.91	−0.15	0.02	−0.23
	2.70	31,400 (7,059)	782 (30.8)	4.18	−0.08	−0.01	1.60
	2.94	32,281 (7,257)	851 (33.5)	4.47	−2.20	0.09	0.45
	3.18	33,362 (7,500)	864 (34.0)	4.33	−0.12	−0.69	−0.17
Actual building models, scaling factor = 1.5	1.03 (R05)	35,061 (7,882)	320 (12.6)	2.54	0.35	−0.20	0.48
	1.51 (R09)	NCP[a]	NCP[a]	NCP[a]	—	—	—
	2.51 (R15)	64,437 (14,486)	668 (26.3)	2.34	2.50	0.22	0.13

[a]NCP = numerical convergence problems.

be added. It should be noted that the proposed procedure has not yet been tested on unsymmetric structural models, very tall buildings, bridges, or dams.

Data Availability Statement

For practical applications, the RTS procedure is available as a MatLAB function, which requires a moderate amount of data to characterize the structure. Ground-motion records are available at http://ngawest2.berkeley.edu/. The design spectrum in Fig. 1 was defined using the US Seismic Design Maps tool, available at http://earthquake.usgs.gov/designmaps/us/application.php?

Acknowledgments

The authors thank Neal Simon Kwong and Eric Thompson for their reviews and constructive comments, which helped improve the technical quality and presentation of this article.

References

Akiyama, H. 1985. *Earthquake-resistant limit-state design for buildings*. Tokyo: University of Tokyo Press.

Arias, A. 1970. "A measure of earthquake intensity." In *Seismic design for nuclear power plants*, edited by R. J. Hansen, 438–483. Cambridge, MA: MIT Press.

ASCE. 2010. *Minimum design loads for buildings and other structures*. ASCE/SEI 7-10. Reston, VA: ASCE.

ASCE. 2013. *Seismic evaluation and retrofit of existing buildings*. ASCE/SEI 41-13. Reston, VA: ASCE.

ASCE. 2016. *Minimum design loads for buildings and other structures*. ASCE/SEI 7-16. Reston, VA: ASCE.

ATC (Applied Technology Council). 2005. *Improvement of nonlinear static seismic analysis procedures*. Rep. No. FEMA-440. Washington, DC: ATC.

Avila, W. 2018. "Reducing of processing time of nonlinear response history analysis of complex structures." M.Sc. thesis, Dept. of Civil and Environmental Engineering, Universidad de los Andes.

Chopra, A. K. 2007. *Dynamics of structures: Theory and applications to earthquake engineering*. 4th ed. Upper Saddle River, NJ: Prentice-Hall.

Chopra, A. K. 2017. *Dynamics of structures: Theory and applications to earthquake engineering*. 5th ed. Upper Saddle River, NJ: Prentice-Hall.

Chopra, A. K., and R. K. Goel. 2004. "A modal pushover analysis procedure to estimate seismic demands for unsymmetric-plan buildings." *Earthquake Eng. Struct. Dyn.* 33 (8): 903–927. https://doi.org/10.1002/eqe.380.

Fajfar, P. 2000. "A nonlinear analysis method for performance based seismic design." *Earthquake Spectra* 16 (3): 573–592. https://doi.org/10.1193/1.1586128.

Hancock, J., J. Watson-Lamprey, N. Abrahamson, J. Bommer, A. Markatis, E. McCoy, and R. Mendis. 2006. "An improved method of matching response spectra of recorded earthquake ground motion using wavelets." *J. Earthquake Eng.* 10 (1): 67–89. https://doi.org/10.1080/13632460609350629.

ICC (International Code Council). 2015. *International building code*. Whittier, CA: ICC.

ICC (International Code Council). 2016. *California building code*. Whittier, CA: ICC.

Malhotra, P. K. 2002. "Cyclic-demand spectrum." *Earthquake Eng. Struct. Dyn.* 31 (7): 1441–1457. https://doi.org/10.1002/eqe.171.

Medina, R. A. 2002. "Seismic demands for nondeteriorating frame structures and their dependence on ground motions." Ph.D. dissertation, Dept. of Civil and Environmental Engineering, Stanford Univ.

Reyes, J. C. 2009. "Estimating seismic demands for performance-based engineering of buildings." Ph.D. dissertation, Dept. of Civil and Environmental Engineering, Univ. of California, Berkeley.

Reyes, J. C., and A. K. Chopra. 2011a. "Evaluation of three-dimensional modal pushover analysis for unsymmetric-plan buildings subjected to two components of ground motion." *Earthquake Eng. Struct. Dyn.* 40 (13): 1475–1494. https://doi.org/10.1002/eqe.1100.

Reyes, J. C., and A. K. Chopra. 2011b. "Three-dimensional modal pushover analysis of buildings subjected to two components of ground motion, including its evaluation for tall buildings." *Earthquake Eng. Struct. Dyn.* 40 (7): 789–806. https://doi.org/10.1002/eqe.1060.

Reyes, J. C., and E. Kalkan. 2011. *Required number of ground motion records for ASCE/SEI 7 ground motion scaling procedure*. USGS Open-File Rep. 2011-1083. http://pubs.usgs.gov/of/2011/1083/.

Reyes, J. C., and E. Kalkan. 2012. "How many records should be used in an ASCE/SEI-7 ground-motion scaling procedure?" *Earthquake Spectra* 28 (3): 1223–1242. https://doi.org/10.1193/1.4000066.

Reyes, J. C., A. C. Riaño, and E. Kalkan. 2015. "Extending modal pushover-based scaling procedure for nonlinear response history analysis of multi-story unsymmetric-plan buildings." *Eng. Struct.* 88 (Mar): 125–137. https://doi.org/10.1016/j.engstruct.2015.01.041.

Reyes, J. C., A. C. Riaño, E. Kalkan, O. A. Quintero, and C. M. Arango. 2014. "Assessment of spectrum matching procedure for nonlinear analysis of symmetric- and asymmetric-plan buildings." *Eng. Struct.* 72 (Aug): 171–181. https://doi.org/10.1016/j.engstruct.2014.04.035.

Todorovska, M. I., H. Meidani, and M. D. Trifunac. 2009. "Wavelet approximation of earthquake strong motion-goodness of fit for a database in terms of predicting nonlinear structural response." *Soil Dyn. Earthquake Eng.* 29 (4): 742–751. https://doi.org/10.1016/j.soildyn.2008.08.001.

Vamvatsikos, D., and C. A. Cornell. 2002. "Incremental dynamic analysis." *Earthquake Eng. Struct. Dyn.* 31 (3): 491–514. https://doi.org/10.1002/eqe.141.

Vamvatsikos, D., and C. A. Cornell. 2004. "Applied incremental dynamic analysis." *Earthquake Spectra* 20 (2): 523–553. https://doi.org/10.1193/1.1737737.

Zhong, P., and F. Zareian. 2014. "Method of speeding up buildings time history analysis by using appropriate downsampled integration time step." In *Proc., 10th US National Conf. on Earthquake Engineering*. Oakland, CA: Earthquake Engineering Research Institute.